Thermochimica Acta
Elsevier Publishing Company, Amsterdam
Printed in Belgium

HIGH-TEMPERATURE THERMAL ANALYSIS OF HIGH BORON ALLOYS USING AUTOMATIC OPTICAL PYROMETRY*

R. W. MAR
Materials Division 8314, Sandia Laboratories, Livermore, Calif. 94550 (U. S. A.)
(Received March 6th, 1972)

ABSTRACT

An automatic optical pyrometer and an induction furnace were used to obtain heating and cooling curves for boron and high boron compounds. Non-variant phase transformations were easily detectable, causing the usual classical thermal arrest shapes on thermal analysis curves. The onset of precipitation of a primary phase in the melt was exaggerated because of a combination of factors affecting the surface, and the liquidus was indicated by a sharp peak on the cooling curve. Using this technique, the melting point of boron was established as 2315 ± 20°K, and erbium dodecarboride was found to melt peritectically at 2356°K.

INTRODUCTION

The classical techniques of differential thermal analysis, heating curve analysis, and cooling curve analysis are difficult to extend to extreme temperatures because of the temperature limitations of the thermal sensor materials. Therefore, the determination of high-temperature phase relationships requires special considerations. The bulk of high-temperature phase diagrams have been established by X-ray and metallographic analysis on samples quenched from various temperatures. However, besides being extremely cumbersome this technique often overlooks high-temperature phase relations due to the unusual kinetics of high temperatures.

This paper presents a simple and relatively inexpensive technique for exploring high-temperature phase relationships, in which an automatic optical pyrometer and an automatically controlled induction furnace are used to obtain thermal analysis curves. The technique is quite sensitive to small effect phase transitions and is also capable of distinguishing between variant and non-variant phenomena. The problems of surface emittance and surface condition, which are so critical in radiation pyrometry, are contended with; in fact, it is demonstrated that these very problems can be used to good advantage in depicting small effect changes.

Efforts to extend thermal analysis techniques to extreme temperatures have

*Presented before the Third Annual Meeting of the North American Thermal Analysis Society in Waco, Texas, on February 7–8, 1972.

tended toward using radiation detectors as thermal sensors[1–6]. Rudy *et al.*[1], Rupert[2,3] and Baldwin *et al.*[6], have designed elaborate high-temperature thermal analysis systems that use photodiode or infrared detector circuits to sense the surface-emitted radiation, while simultaneously measuring the temperature with a conventional pyrometer. While the experimental setup described here does not differ in principle, in practice it is much simpler, thus minimizing the necessary equipment and circuitry. The thermal-sensing and temperature measurement functions are one in the same: the output from a commercially-available optical pyrometer.

Previous investigators[1,3,6] have never pursued the prime advantage of heating and cooling curves, namely the differentiation of phase transition type by characteristic curve shapes. Instead, emphasis has been on the use of differential thermal analysis, derivative thermal analysis, and thermal derivative thermal analysis treatments to magnify the occurrence of phase changes. The extent to which characteristic thermal arrest shapes can be used to identify types of phase changes is explored here. To illustrate the technique, the salient features of heating and cooling curves for congruent melting, precipitation, and peritectic and eutectic transformations of boron and high boron compounds are discussed.

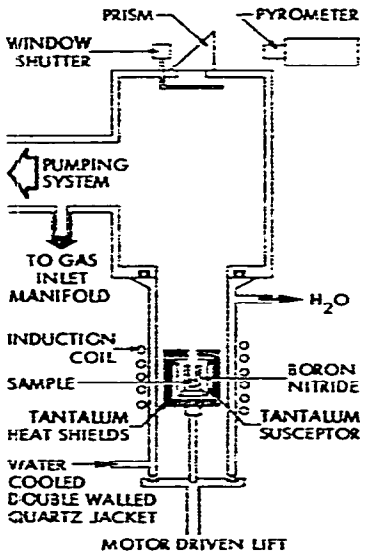

Fig. 1. Schematic of the experimental setup.

EXPERIMENTAL

A schematic diagram of the experimental setup is shown in Fig. 1. Heating was done in an induction furnace capable of operating at vacuums of 10^{-5} torr or in controlled atmospheres. A tantalum crucible with a lid was used as the susceptor. The crucible was well shielded by a number of 0.002-in. thick tantalum shields, and was supported on a rod and pedestal made of tantalum. The vacuum chamber con-

sisted of a double-walled quartz jacket through which cooling water flowed. The induction coils were exterior to the quartz jacket, and were connected to a 15-kw, 10-kHz motor generator. Power to the coils could be increased and decreased automatically at desired rates by a power controller connected to the generator.

A Pyro automatic optical pyrometer was used to determine heating and cooling curves. The sample was observed through a calibrated window and prism, and through concentric orifices in the radiation shielding and susceptor lid. The pyrometer output was recorded directly on a strip chart recorder. The pyrometer output was about 0.1 mV/degree, and the recorder sensitivity could be selected by the appropriate range selection and zero suppression circuitry.

The samples were crystalline boron and high boron alloys prepared by arc melting crystalline boron of 99.96% purity with the metal of choice. Erbium sponge of 99.9% purity and uranium chips of 99.9% purity were used as starting materials.

Boron nitride crucibles were used because it was found that boron and high boron alloys could be melted in these crucibles with no sample–crucible interactions. The dissociation of boron nitride to nitrogen gas and solid or liquid boron is significant above 2000°C[7]; therefore, catastrophic dissociation was prevented by performing the experiments in 10 p.s.i. argon. The boron nitride crucibles were pre-treated by heating slowly to 1600°C while maintaining a vacuum of $<10^{-4}$ torr, and then heating to 2000°C in argon. Crucibles not treated in this manner caused severe deterioration of the sample, presumably due to the interaction of boron oxide (used as a binder during the hot pressing of boron nitride) with the sample.

The dimensions of the boron nitride crucibles were 7-mm diameter by 3.5-cm high with side walls 1.5-mm thick, and the sample amounts used were typically on the order of 0.1–0.5 cm^3. These crucible dimensions and sample amounts were chosen to meet three criteria.

1. Because radiation pyrometry was used as the thermal sensor, attempts were made to minimize the effects of unknown surface emissivity and surface conditions. Therefore, very small sample volumes were placed at the bottom of a deep, narrow crucible well, thereby simulating near blackbody conditions, and reducing surface condition effects. An emittance of unity was assumed for the pyrometer output.

2. The pyrometer sensed radiation from a 6-mm diameter target area when focused on the sample in the 7-mm diameter crucible cavity; therefore the temperature was representative of the average cavity temperature.

3. To insure that the crucible cavity temperature was indeed representative of the sample temperature, the crucible walls were made as thin as possible to reduce the crucible mass-to-sample mass ratio.

The pyrometer was calibrated against a NBS-calibrated tungsten strip lamp. The greatest uncertainty in the temperature measurement arises from unknown emittances. Because the pyrometer was focused into a deep cavity with a length-to-diameter ratio of 5, blackbody conditions were assumed. The total uncertainty in the temperature measurement is believed to be less than ± 10°C.

The general procedure was to load a pretreated boron nitride crucible with a

few arc-melted sample chips, and then heat to 1600°C in vacuum. During this period the pyrometer was aligned to sight down into the crucible cavity, ensuring that the pyrometer spot size was entirely within the inner crucible diameter. The sample chips could be distinguished only immediately after the power was increased, and this is interpreted as verification that criterion (*1*) above was met. After heating to 1600°C, 10-p.s.i. argon was introduced, and the temperature was increased to 1950°C and held for 5–10 min. Then the power was increased automatically at a controlled power change rate, and a sample temperature–time history was recorded. The cooling curves were obtained by allowing the sample to equilibrate at the maximum temperature for about 10 min, and then decreasing the power automatically to below red heat.

The heating and cooling rates were about 20°C/min, which corresponded to the minimum power rate change setting. The heating and cooling rates were dependent not only upon the rate at which power was supplied to the induction coils, but also to some extent on the efficiency of the susceptor radiation shielding. Therefore, the rates varied slightly from run to run because of shield deterioration.

RESULTS AND DISCUSSION

Heating and cooling curves for boron and various erbium–boron and uranium–boron alloys were obtained to illustrate the characteristic curve features associated with various types of phase transformations. The heating and cooling curves of an empty boron nitride crucible were obtained to determine the effect of a dissociating crucible. The curves were smooth and void of large fluctuations despite the fact that some surface dissociation was occurring at temperatures greater than 2000°C. The effect of changes in the surface were apparently diminished by the deep crucible cavity.

Congruent melting and freezing

The heating and cooling curves for congruently melting crystalline boron are shown on Figs. 2 and 3, respectively. The cooling curve was similar to a classically determined curve, and was characteristic of too little sample and too rapid a cooling rate[8,9]. The thermal arrest was not isothermal, and the features were rounded. Nevertheless, the fusion phenomenon is clearly indicated. Upon cooling, there was supercooling of 10°C, and then a peak temperature of 2030°C was reached. The features of the heating curve were less pronounced, but could be accentuated by plotting the derivative of the curve (based on time increments of 0.2 min) *vs.* time.

The melting point of boron is established as 2042 $\pm$20°C in this investigation, determined by a linear extrapolation of the thermal arrest plateau to the cooling curve. The uncertainty is primarily due to the non-ideal thermal arrest shapes, and possible deviations from blackbody conditions.

Experimentally determined melting points are widely scattered, varying from 2000 to 2400°C (see Table I). The divergence of reported melting points probably reflects not only inaccuracies in experimental procedures, but also the variations in purity and structure of boron. Previous determinations were based primarily upon

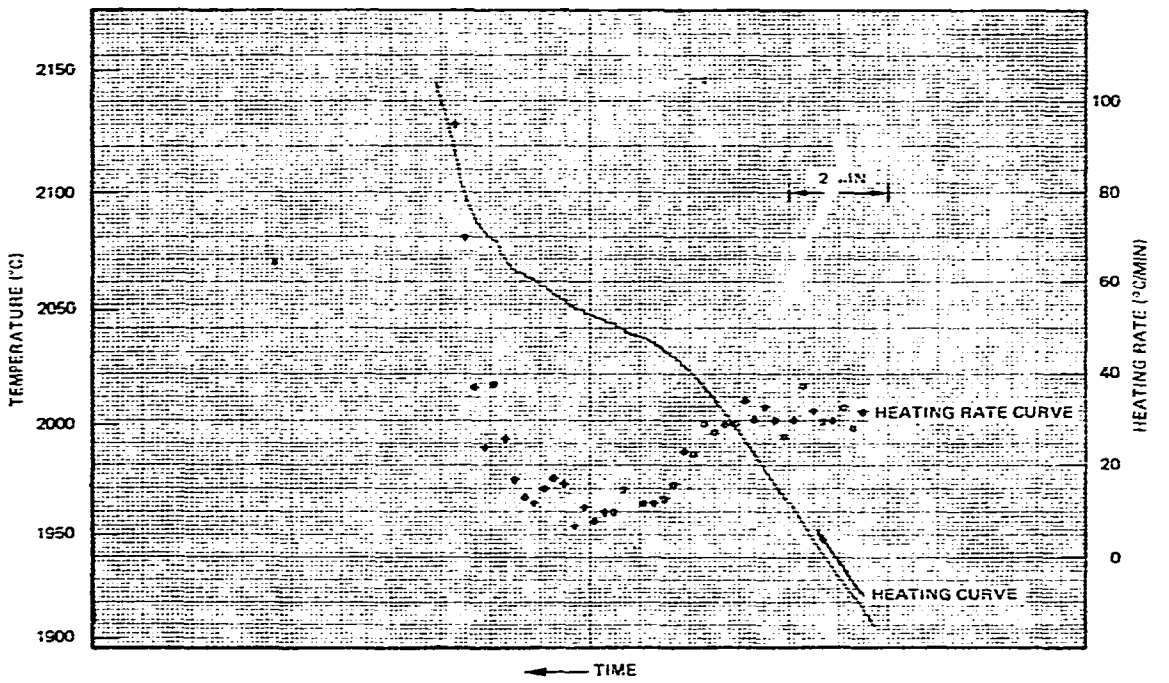

Fig. 2. Heating curve and derivative heating curve for pure crystalline boron.

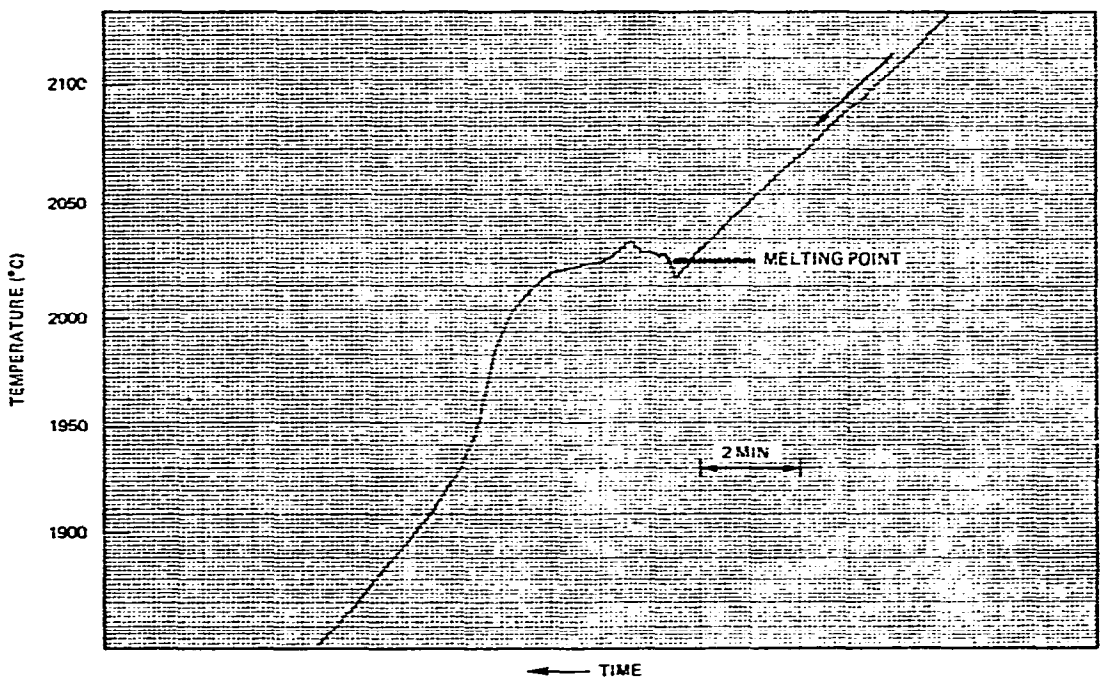

Fig. 3. Cooling curve for pure crystalline boron.

analysis during heating, whereas it has been shown here that the cooling curve is much more reliable. The boron starting purity and structure were 99.96% and β-rhombohedral. Postmelt analyses showed no structural changes, and an increase in nitrogen of about 1500 p.p.m.

TABLE I

REPORTED MELTING POINTS OF BORON

Reference	*Melting point (°K)*
Weintraub, 1913[10]	2673
Tride and Birnbrauer, 1941[11]	2473
Cueilleron, 1944[12]	2313
Cueilleron, 1945[13]	2273–2448
Cooper, 1954[14]	2373–2473
Searcy and Myers, 1957[15]	>2420
Cline, 1959[16]	2403
This investigation	2315

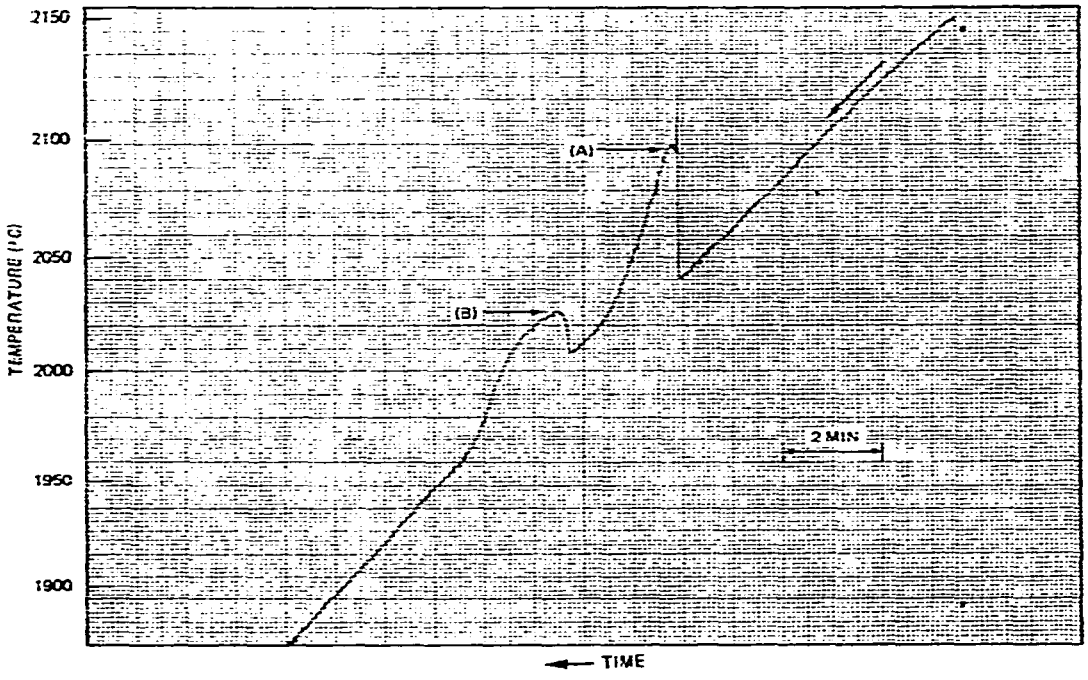

Fig. 4. Cooling curve for 42% uranium–58% boron composition. Point (A) is the onset of precipitation and (B) is a eutectic thermal arrest.

Liquidus and eutectic phenomenon

The precipitation of a primary phase in a melt causes a spiked rise on the cooling curve. For example, Fig. 4 shows the cooling curve for a composition of UB_{30}. The first peak at 2094°C is due to the onset of precipitation of UB_{12}, and a eutectic thermal

arrest at 2025°C is seen. This interpretation was confirmed by the metallographic analysis of the microstructure and the analysis of numerous other compositions. The high degree of supercooling makes it difficult to assign a temperature to the liquidus; however, the presence of two events is unmistakable. The erbium–boron system was found to behave similarly, as seen on Fig. 5. The composition ErB_{25} shows the precipitation of ErB_{12} at 2042°C (peak temperature) and a eutectic reaction at 2010°C. A typical hypereutectic microstructure has been observed for this composition.

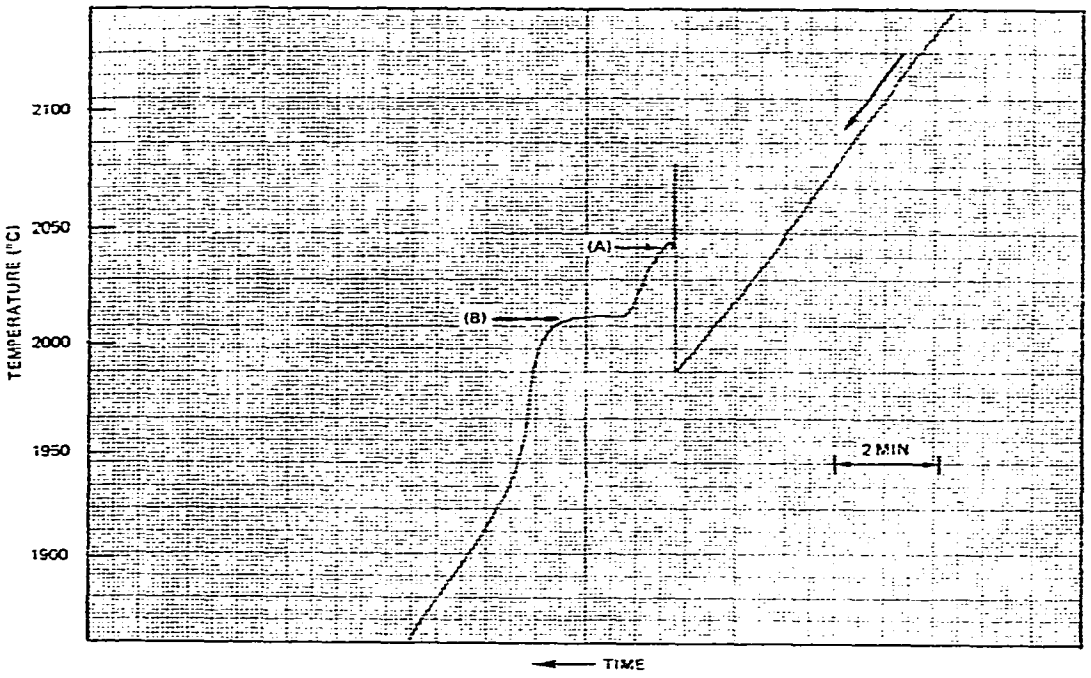

Fig. 5. Cooling curve for 38% erbium–62% boron composition. Precipitation of ErB_{12} occurs at (A) and a eutectic reaction at (B).

The sharp and definitive nature of the liquidus peaks shown on these curves deserves comment. Conventional cooling curves using thermocouples and cooling rates on the same order of magnitude as those used here usually depict the onset of a primary phase precipitant as a change in slope, and this effect is often overlooked experimentally[15]. However, as seen on Figs. 4 and 5, with the optical pyrometer technique, the liquidus event is sharp and unmistakable. No efforts were made to promote supercooling and yet primary supercooling of 50°C was not uncommon. It is felt that the liquidus peak effect is not due entirely to the supercooling tendencies of high boron compositions but is promoted to some extent by the nature of the experimental technique. The technique is immediately sensitive to changes in the sample, and thermal lag, which is common to thermocouple-sensed curves, is eliminated. The precipitation of a primary phase nucleates at the surface and the accompanying thermal

effects are concentrated there, rather than distributed throughout the bulk. Emissivity changes may be occurring as the primary phase forms as well. These effects make surface-emitted radiation extremely sensitive to reactions associated with the liquid–gas interface, and, therefore, the liquidus reaction is accentuated. As the composition is altered in the direction of less precipitate, the liquidus peak diminishes in size. Eventually, the initial spike is lost, and the formation of a small amount of precipitate is represented by a "bump" on the cooling curve. The sensitivity of this technique to the liquidus event upon cooling has been extremely useful in elucidating the fusion nature of erbium dodecaboride, as discussed below.

In general, the heating curves were only useful for indicating non-variant phase transformations. The heating curves for both UB_{30} and ErB_{25} resembled the curve for pure boron (Fig. 2), failing to differentiate between the non-variant phase transformation, the two-phase region of primary phase and liquid, and the complete molten state.

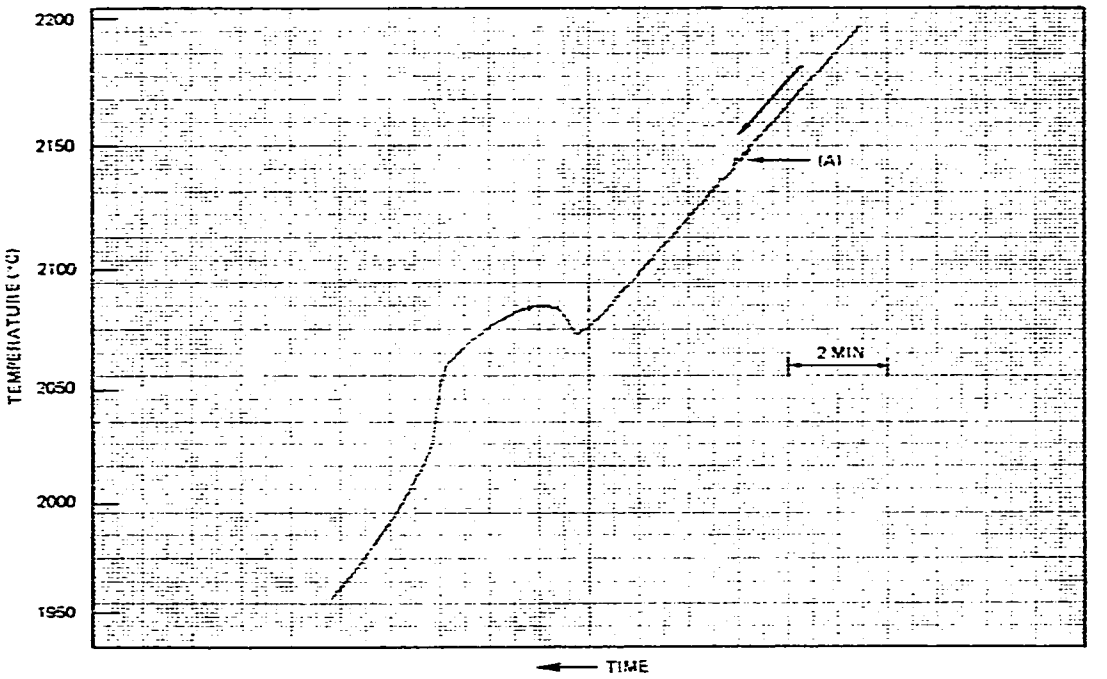

Fig. 6. Cooling curve for $ErB_{12.6}$. A possible phase transition is shown at (A).

Peritectic phenomenon

The cooling curve of $ErB_{12.6}$ is shown in Fig. 6. The major event is a thermal arrest which occurs at a peak temperature of 2083 °C, after a supercooling by about 10 °C. It was felt that the very small perturbation in the cooling curve at 2145 °C, was not just some spurious effect, but was indicative of a phase reaction. To further explore this event, the cooling run was repeated with the boron nitride crucible half filled with sample, thereby, increasing the surface effects and reducing the blackbody cavity

effect. In the resulting cooling curve, shown in Fig. 7, the high-temperature transition has been reproduced and magnified indicating that it most certainly represents a phase transition of some sort. This effect is interpreted as being due to the precipitation of a primary phase at the surface, the dissolution or gravitational mixing into the bulk, and repeated precipitation. Therefore, the cooling curves on Figs. 6 and 7

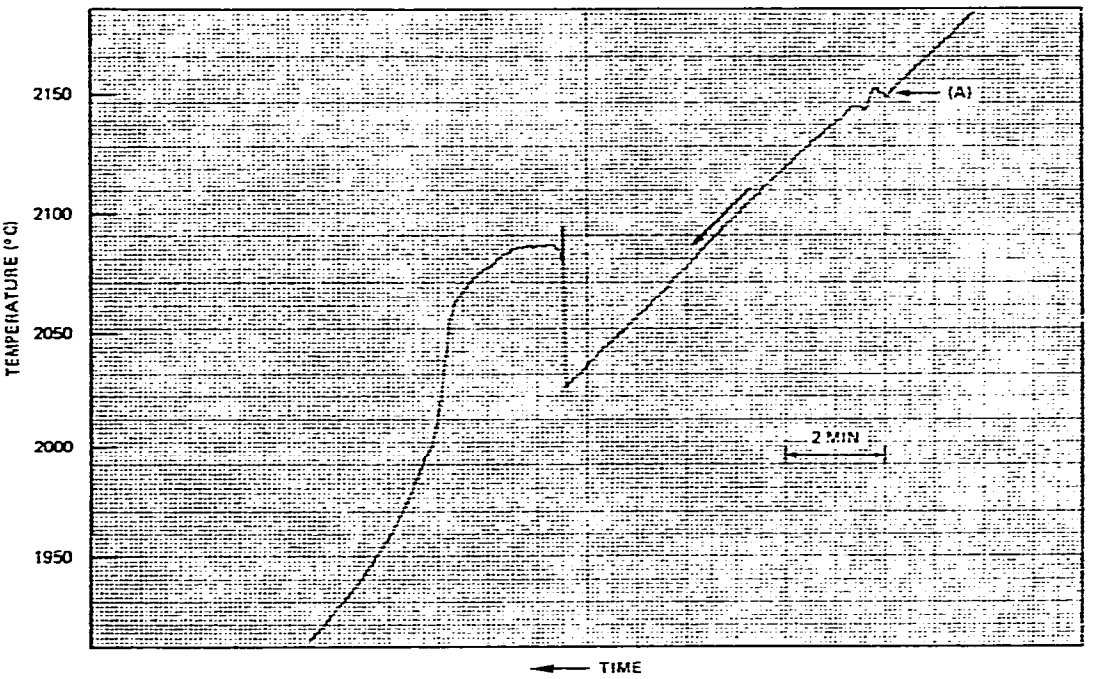

Fig. 7. Cooling curve for $ErB_{12.6}$ (crucible filled one-half full). Point (A) shows the same phase transition noted in Fig. 6.

show a liquidus event at 2145 °C and a non-variant reaction at 2083 °C, which is the peritectic freezing of erbium dodecaboride. The liquidus effect in $ErB_{12.6}$ was very small (compare Figs. 5 and 6), and it is doubtful whether conventional techniques would have detected the change.

CONCLUSIONS

It has been demonstrated that a simple experimental setup using an automatic optical pyrometer can be used as a sensitive thermal analysis system. The occurrence of phase transitions can be prominently identified by the treatment (derivative, thermal derivative, etc.) of heating and cooling curves. Under the conditions used in these experiments the cooling curves were much more informative than the heating curves in that the irregularities signifying phase transitions were considerably more apparent on the cooling curve. It has been shown that variant phase reactions and non-variant phenomenon can be distinguished from each other by their characteristic shapes on

the cooling curve. Non-variant reactions show up as isothermal arrests similar to the usual classical shapes, whereas the liquidus transition appears as a sharp peak. It was found that the technique was extremely sensitive to the liquidus event.

ACKNOWLEDGEMENTS

The author gratefully acknowledges the advice and assistance given by Norman D. Stout (L. L. L.) in setting up the experiment and interpreting the results. Equipment and apparatus were kindly made available by the Lawrence Livermore Laboratory high-temperature chemistry group.

REFERENCES

1 E. Rudy, H. D. Heederke, and T. Eckert, *Ternary Phase Equilibria in Transition Metal–Boron–Carbon–Silicone Systems, Tech. Rep. No. AFWL-TR-65-2*, Part III, Vol. I, May 1965.
2 G. N. Rupert, *Rev. Sci. Instrum.*, 34 (1963) 1183.
3 G. N. Rupert, *Rev. Sci. Instrum.*, 36 (1965) 1629.
4 E. K. Storms and R. J. McNeal, *J. Phys. Chem.*, 66 (1962) 1401.
5 E. K. Storms and N. H. Krikorian, *J. Phys. Chem.*, 64 (1960) 1471.
6 N. L. Baldwin, S. Langer, F. L. Kester, and C. Hancock, *Rev. Sci. Instrum.*, 41 (1970) 200.
7 D. L. Hildenbrand and W. F. Hall, *J. Phys. Chem.*, 67 (1963) 888.
8 W. Hume-Rothern, J. W. Christian, and W. B. Pearson, *Metallurgical Equilibrium Diagrams*, The Institute of Physics, London, 1952.
9 F. N. Rhines, *Phase Diagrams in Metallurgy—Their Development and Application*, McGraw–Hill, New York, 1956.
10 E. J. Weintraub, *Ind. Eng. Chem.*, 5 (1913) 106.
11 Tride and Birnbrauer, *Z. Anorg. Allgem. Chem.*, 87 (1941) 129.
12 J. Cueilleron, *Ann. Chim.*, 19 (1944) 459.
13 J. Cueilleron, *Compt. Rend.*, 221 (1945) 698.
14 H. S. Cooper, in C. A. Hampel (Ed.), *Rare Metals Handbook*, Reinhold, New York, 1954.
15 A. W. Searcy and C. E. Myers, *J. Phys. Chem.*, 61 (1957) 957.
16 C. F. Cline, *J. Electrochem. Soc.*, 106 (1959) 332.